ENHANCEMENT OF EVAPORATION OF FALLING LIQUID FILM ON HORIZONTAL TUBE BUNDLE

Mostafa M. Awad* and El-Sayed R. Negeed**

* Mechanical Power Dept., Faculty of Engineering, Mansoura University, Egypt
E-mail: mostawad100@yahoo.com
** Reactors Dept., Nuclear Research Center, Atomic Energy Authority, Cairo, Egypt

ABSTRACT

Enhancement of the evaporation heat transfer coefficient is important for the design and operation of horizontal tube spray film evaporators. Water spray on a horizontal tube bundle is numerically and expermentally studied in steady state condition. The objective of the present study is to evaluate the evaporation rate of falling liquid film on the horizontal tube bundle and obtaining the best distance between the nozzle and the upper evaporator tube. Moreover, the effect of falling Reynolds number, subcooled inlet sprayed water, evaporation pressure, and hot tube surface superheating on the evaporation rate are also analyzed.

An experimental test loop was installed where the used nozzle is of a fan-jet flat nozzle type, which is usually used in evaporation and desalination processes. By using the phase / doppler particle analyzer, the droplet velocity and the droplet size were measured.

The non-dimensional governing equations of mass, momentum and energy of the created liquid film around the hot tube surface are solved numerically using the finite difference method. Therefore, the model can precisely predicts the layer thickness, velocity profile, temperature distribution, and local and average heat transfer coefficients of the formed film. The results show that, the evaporation rate and Nusselt number are mainly increased by increasing the surface temperature and also, by increasing the tube outer diameter. Decreasing the chamber pressure, inlet liquid subcooling and falling Reynolds number result in increase in the evaporation rate and Nusselt number. The falling distance has a little influence on the evaporation rate and Nusselt number. Comparing the experimental results with the theoretical ones, gives a good agreement between them with an acceptable difference ranges from 8 to 15%. An empirical correlation has been deduced describing the relation between the average heat transfer coefficient of the outside film around the heated tube evaporator and the following affecting parameters; feed liquid rate, heat flux, falling distance from the nozzle to the hot tube surface, falling liquid temperature and the hot tube surface temperature.

Keywords: Spray cooling hot surface, liquid film evaporation upon horizontal tube evaporator.

NOMENCLATURE

A_o Test tube outer surface area, m^2
Cp Specific heat at constant pressure, *J/kg.K*
D Differentiation sign
d_1 Droplet initial diameter, *m*
d Droplet diameter after falling distance, *m*
d_{ot} Test tube outer diameter, *m*
g Acceleration due to gravity, m^2/s
h' Average heat transfer coefficient, W/m^2K
L Test tube length, *m*
LH Latent heat for vaporization, *J/kg*
m'_w Sprayed mass flow rate, *kg/s*
m'_v Evaporation rate, *kg/s*
p Pressure, N/m^2
p_{spr} Spray pressure, N/m^2
q Heat flux, W/m^2
Q_t Transmitted heat, *W*
r radius, *m*
t_1 Sprayed water inlet temperature, *K*
t_2 Droplet temperature after the falling distance, *K*
t_w Temperature of the test tube outer surface, *K*
t_s Evaporation temperature, *K*
V Volume, m^3
v Velocity, *m/s*
v_1 Droplet initial velocity, *m/s*
v_2 Droplet velocity after the falling distance, *m/s*
ZZ Droplet falling distance (vertical distance from the nozzle to the test tube surface), *m*

Greek letters

Γ Sprayed mass flow rate per one side of the hot tube surface, *kg/s.m*
$\Delta t_{sup.}$ Superheating (the difference between the hot surface temperature and the formed vapor saturation temperature), *K*
$\Delta t_{sub.}$ Subcooling (the difference between the formed vapor saturation temperature and the sprayed water initial temperature), *K*
δ Liquid layer thickness, m
φ_n Nozzle angle, *deg.*
μ Dynamic viscosity, $N.s/m^2$
ρ Density, kg/m^3
τ Time, *s*

Subscripts

f Liquid film
1 Initial value

v Vapor
w Water
zz At the falling distance zz

Abbreviations

P/DPA Phase / Doppler Particle Analyzer
η_{ev} Evaporation rate ratio (the ratio between the evaporation rate and the initial sprayed mass flow rate)

Dimensionless numbers

Nu Nusselt number, $= h\, d_{ot} / k_f$
Pr Prandtl number, $= Cp\, \mu_f / k_f$
Re Reynolds number, $= u_r\, r\, \rho_w / \mu_w$
Re_f Falling Reynolds number, $= 4\, \Gamma / \mu_w$

1. INTRODUCTION

1.1. General

Heat transfer through falling film or spray film evaporation has been widely employed in heat exchange devices which are used in many applications i.e. desalination and ocean thermal energy conversion (OTEC) system. The horizontal tube spray film evaporators have been proposed to operate at the available small temperature difference. These evaporators basically consist of a bundle of horizontal tubes connected by headers at each end, as in the conventional shell and tube heat exchangers. The shell side liquid is introduced through spray nozzles to the top of the bundle and falls from tube to another. Liquid films flow and evaporate on the outside tube surfaces. The principal advantages of spray film evaporators are high heat transfer rates at small temperature differences and small liquid inventory.

1.2. Droplet - hot surface impact

The maximum spread of a droplet upon impact on a hot surface, depends mainly on the liquid viscosity and liquid-surface contact angle, while, the tendency of a droplet to deposit or rebound is determined primary by the droplet impinging speed and hot surface temperature. This will create a liquid film on the evaporator tube surface that has a direct effect on the heat transfer coefficient and on the evaporation rate. The evaporator effectiveness will depend on how the liquid film falls from one tube to another. As the flow rate varies, three basic flow patterns may be observed: discrete droplets, jets or continuous sheet, Wei and Jacobi [1]. At a very low flow rate, the liquid departs from the bottom of the tube in droplet mode. A gradual increase in the flow rate can cause a transition from droplets to jets, where at higher flow rates a transition will be from jets to a liquid sheet. Hu and Jacobi [2] provided the first generalized flow-pattern maps for predicting falling-film mode. The map includes the

different modes. It should be noted that in the present study the liquid sheet falling between horizontal tubes mode is considered.

1.3. Scope of the present study

The main objective of this study is improving the evaporation rate in the horizontal tube evaporators by spraying water upon the hot surfaces. The present analytical work studies the effect of liquid film formation, droplets density, droplet size distribution, hot tube surface temperature, falling distance and the inlet spray subcooling on the heat transfer coefficient and evaporation rate.

2. EXPERIMENTAL WORK

2.1. Experimental setup

The schematic diagram of the experimental setup is shown in Fig. (1). This setup consists of a test chamber (1), primary heater (9), first electrical heater (10), second electrical heater (11), hot water distributor (5), calibrated tank (6), condenser (7), condensate tank (8) and circulating pump (15). The spray water temperature is controlled and regulated by a primary condensing vapor heater (9) and two electrical heaters (10,11). The water is then introduced to the test section through the spray nozzles that give a spray flat-film upon the tube bundle. This bundle is heated by dry saturated steam to obtain constant surface temperature during the experiments. A fire tube boiler with a capacity of 2 ton/hr saturated or superheated steam at maximum pressure 10 bar is used for this setup. The boiler and the setup are located in Heat Transfer Laboratory, Reactors Department, Nuclear Research Center. The heating steam from the boiler passes through the evaporator and condensed in condenser (7) where its flow rate is measured by the collecting tank (8). Liberated vapor from the test chamber condenses in the primary heater (9) and its condensate is collected and measured by the aim of calibrated tank (13). The non-evaporated spray water is collected and measured in tank (6).

2.1.1. The test chamber

As shown in Fig. (2), the stainless steel test chamber has nominal dimensions of 40 x 50 x 90 cm and wall thickness of 5 mm. It accommodates water tube header, nozzles, and in-line tube bundle. There are two Pyrex windows of 25 cm diameter for visual observation of the boiling phenomenon and sprayed water characteristics and for the use of P/PDA to measure the velocity and size of droplets. The falling distance is adjusted by moving the distributor up and down through two grooves on the top of the test chamber. Water enters the test chamber through the nozzles distributor at a temperature as near as possible to the saturation temperature corresponding to the pressure inside the test chamber.

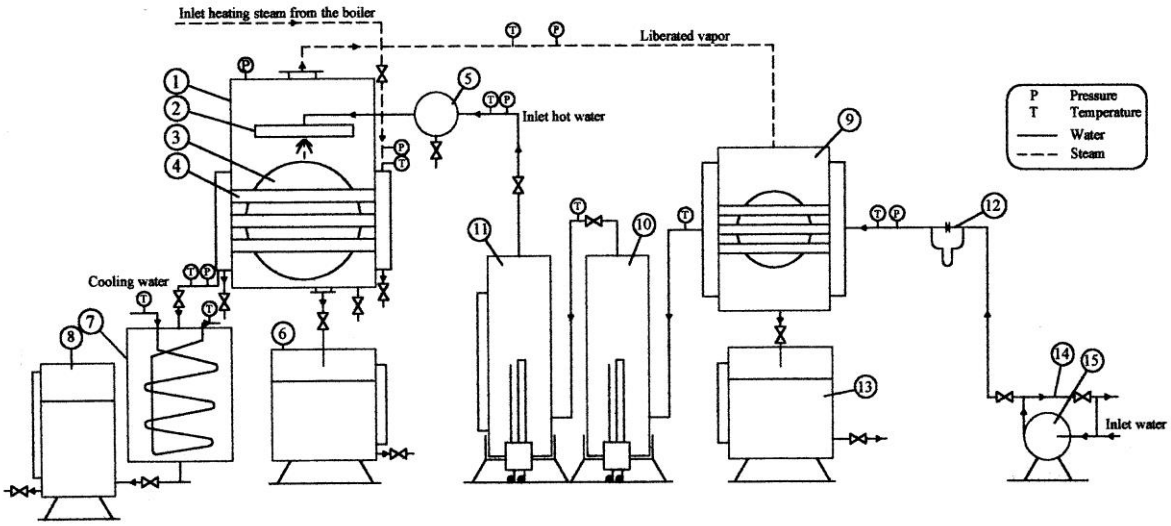

1. Test chamber
2. Nozzles distributor
3. Pyrex windows
4. Test tubes
5. Hot water distributor
6. Calibrated tank
7. Condenser
8. Condensate tank
9. Primary tank
10. First electrical heater
11. Second electrical heater
12. Orifice meter
13. Calibrated tank
14. By-bass line
15. Circulating pump

Fig. (1). Line diagram of the experimental setup.

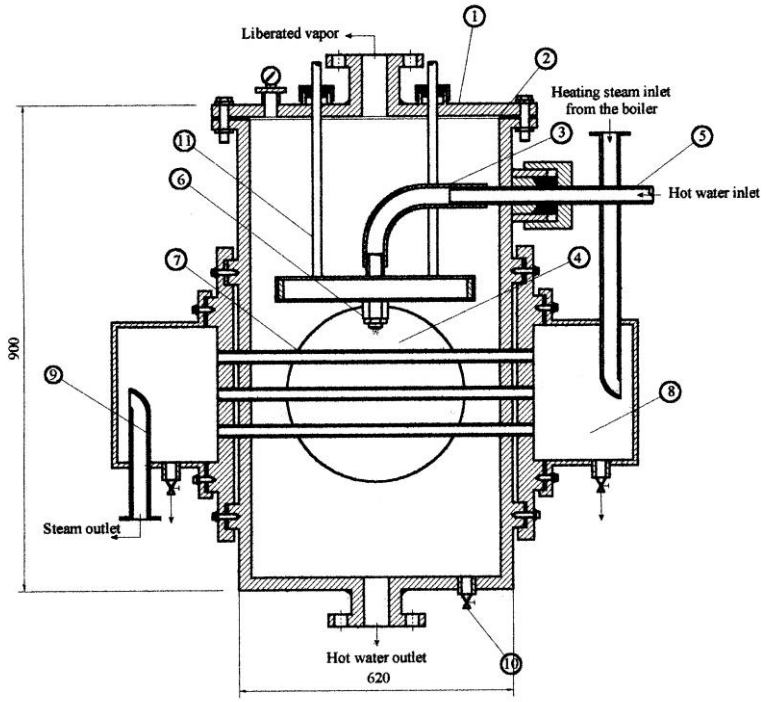

1. Demister plate
2. Rubber gasket
3. Rubber tube
4. Pyrex windows
5. Three channels
6. Three spraying nozzles
7. Nine testing tubes
8. Inlet steam chamber
9. Outlet steam chamber
10. Vent valve
11. Nozzles distributor carrier

Fig. (2). Sectional view of the test chamber.

2.1.2. Spraying nozzles

Three spraying nozzles were set up for spraying water over the tube bundle. The used nozzles are of fan-jet flat-spray type manufactured by Steinen Co., U.S.A. The nozzle is constructed from four main parts: Cap, orifice tip, strainer with 100-mesh stainless steel screen and adapter.

2.1.3. Inline evaporator tubes bundle

The tube bundle contains 9 stainless steel tubes, arranged in an inline form in three columns and three rows. The tubes are arranged with a transverse (horizontal) pitch equals to 3.5 of test tube outside diameter, while the longitudinal (vertical) pitch equals to 1.8 of outside diameter.

2.2. Measurements

2.2.1. Droplet velocity and size measurement

The droplet velocity and size were measured by using an Aerometric Phase / Doppler Particle Analyzer (P/DPA). It utilizes light scattering from two laser beams, at its intersection point, by spherical particles to obtain a simultaneous size and velocity measurements for individual particles. As shown in Fig. (3), the P/DPA consists of four main components; the transmitter, receiver, signal processor and computer.

2.2.2. Liquid layer thickness around the hot surface measurement

The formed liquid layer thickness around the hot tube surface is measured by using an electric film thickness-measuring probe. This probe, as shown in Fig. (4), consists of a depth micrometer, a spatial mechanism to transfer the rotating movement of the micrometer to axial movement, and an electric contact circuit to show the film thickness.

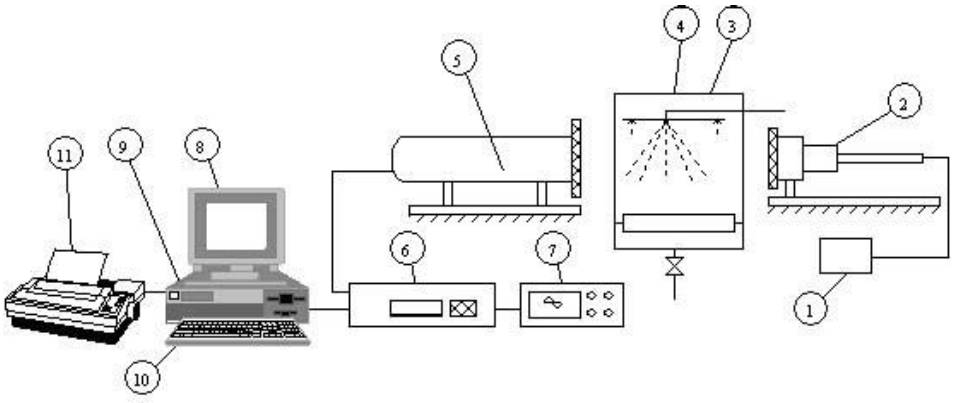

1. Exciting power supply
2. Laser beams transmitter
3. Nozzle distributor
4. Test chamber
5. Receiver
6. P/PDA signal processor
7. Oscilloscope
8. Monitor
9. Computer C. P. U.
10. Key board
11. Printer

Fig. (3). Schematic diagram of the phase doppler particle analyzer, (P/DPA).

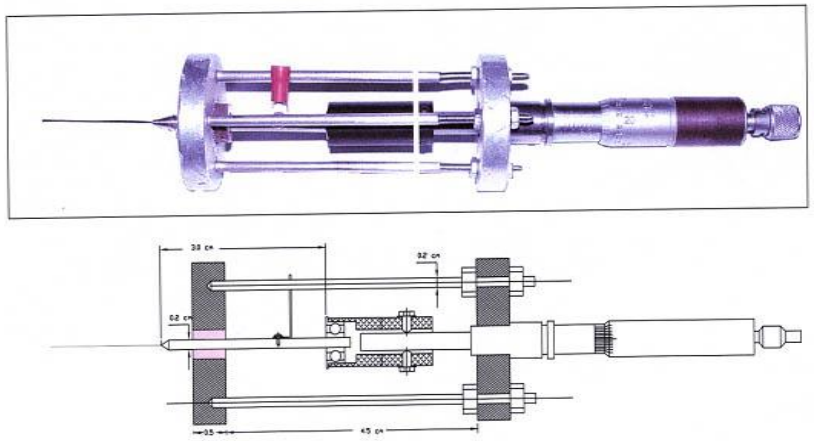

Fig. (4). Film thickness measuring probe.

3. MATHEMATICAL MODEL

3.1. Governing equations for the region from the nozzle up to the droplet formation.

The plane liquid sheet is consider to have uniform thickness w_s, discharged from a two dimensional nozzle, as shown in Fig. (5).

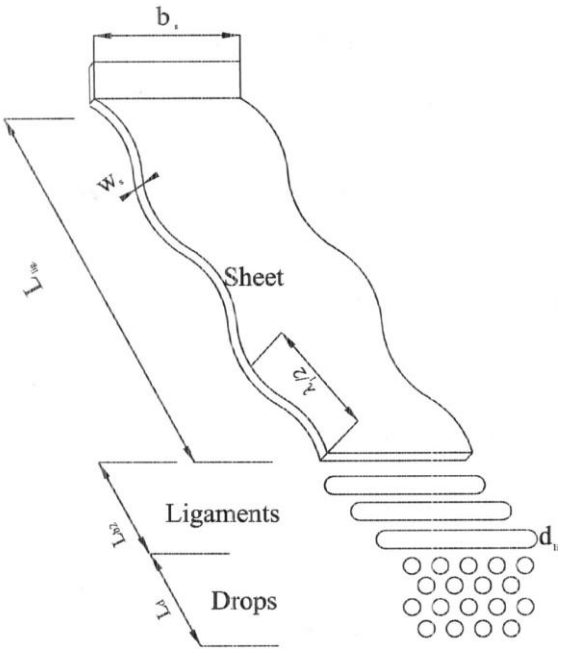

Fig. (5). Schematic of a plane liquid sheet breakup leading to spray formation.

In order to simplify the model for the breakup of the liquid sheet, the following assumptions were made; isothermal process, no mass transfer between the liquid sheet and the surrounding, the liquid sheet thickness is constant, the growth of unstable waves on the liquid sheet is sinusoidal which will eventually break the liquid sheet into ligaments, two dimensional model, viscous and incompressible liquid sheet moves with velocity u_s through a quiescent incompressible medium, wave amplitude of the liquid sheet is small except very close to the breakup point and the liquid sheet is flat as suggested by Dombrowski and Johns [3]. The growth of unstable sinusoidal waves on the liquid sheet is similar to the model proposed by Dombrowski and Johns [3].

Assuming that a spectrum of infinitesimal disturbances are imposed on the initially steady motion, (i.e. the instability produced fluctuating velocities and pressures for both the liquid sheet and the surrounding vapor) and have the following form:

$$\eta = \eta_0 \exp(iKzz + \Omega\tau) \tag{1}$$

Where Ω is the complex growth rate, $\Omega = \Omega_r + i\,\Omega_i$.

The most unstable disturbance has the largest value of Ω_r, denoted by Ω_{max}, and is assumed to be responsible for liquid sheet breakup. The resulting ligament size is related to the maximum unstable wavelength $\lambda_1 = 2\pi/K_1$ where K_1 is the wave number corresponding to the maximum growth rate Ω_{max}.

Senecal et al. [4] derived a relation for the unstable sinuous waves on an incompressible liquid sheet flowing in an incompressible gas medium. The resulting expression for the most unstable disturbance, Ω_r, is given as follows:

$$\Omega_r = (\rho u_s^2 K^3 (\frac{w_s}{2}) - \frac{\sigma K^3}{\rho_w (K(\frac{w_s}{2}) + \rho)})^{\frac{1}{2}} / (K(\frac{w_s}{2}) + \rho) \tag{2}$$

where:

u_s is the total sheet velocity, $u_s = (2\Delta p/\rho_w)^{1/2}$,

Δp is the spray pressure difference,

w_s is the sheet thickness at breakup which was derived by Fraser et al. [5] as:

$$w_s = (\frac{1}{2[\ln(\eta_b/\eta_0)]^2})^{\frac{1}{3}} (\frac{(FN)^2 \rho_v u_s}{\rho_w \sigma})^{\frac{1}{3}} \tag{3}$$

and FN is the spray nozzle parameter, which can be derived by Fraser et al. [5] as:

$$FN = \frac{m_w'}{(\rho_w \Delta p)^{1/2}} \tag{4}$$

Dombrowski and Johns [3] demonstrated that the quantity $\ln(\eta_b/\eta_0)$ is equal to 12.

According to Rayleigh's theory [6], the most unstable wave is the one with the maximum growth rate which occurs at the dominant wavelength λ_1 obtained from:

$$\frac{D\Omega_r}{DK} = 0.0 \tag{5}$$

From Equations (2) and (5), the values of the wave number (K_1) corresponding to the maximum growth rate, $\Omega_{max.}$, can be evaluated. Then, wavelength (λ_1) can be calculated from:

$$\frac{D\Omega_{rw}}{DK} = 0.0 \tag{6}$$

The physical mechanism of sheet disintegration proposed by Dombrowski and Johns [3] is adopted in order to predict the drop sizes produced from the primary breakup process. Ligaments are assumed to form from the sheet breakup process once the unstable waves reach the critical amplitude. The onset of ligament formation, or liquid sheet breakup length, can be formulated based on analogy with the breakup length of cylindrical liquid jets. If the surface disturbance has reached a value of η_b at breakup time, τ_{b1}, where the liquid sheet will breakup and ligaments will be formed, it can be presented using Equation (1), and noting that the value of the imaginary part of a complex growth rate (Ω_i) equals zero at the breakup, Dombrowski and Johns [3], then:

$$\eta_b = \eta_0 \exp(\Omega_{max.}\tau_{b1}) \quad \text{or} \quad \tau_{b1} = \frac{1}{\Omega_{max.}}\ln(\frac{\eta_b}{\eta_0}) \tag{7}$$

where $\Omega_{max.}$ is the maximum growth rate, found by numerically maximizing Equation (2) as a function of K.

Thus the sheet will breakup and ligaments will be formed at a length, $L_{lig.}$, given by:

$$L_{lig.} = u_s\tau_{b1} = \frac{u_s \ln(\eta_b/\eta_0)}{\Omega_{max.}} \tag{8}$$

3.2. Change in droplet velocity, size and its temperature.

The droplet is exposed to many forces in the region between the nozzle and the tube surface:

The gravitational force which is:

$$F_1 = \frac{g\pi d^3 \rho_w}{6} \tag{9}$$

The buoyancy force which is:

$$F_2 = \frac{\pi g d^3 \rho_v}{6} \tag{10}$$

The drag force which is:

$$F_3 = \frac{C_D \pi d^2 \rho_v (v_w - v_v)^2}{8} \tag{11}$$

The coefficient of drag force (C_D) can be calculated from the following relation (Tanaka drag law) by Linn et al. [7]:

$$\begin{aligned} C_D &= \frac{24}{Re_d} && \text{for } Re_d < 2 \\ &= \frac{10}{Re_d} && \text{for } 2 < Re_d \leq 500 \\ &= 0.44 && \text{for } 500 \leq Re_d < 10^5 \end{aligned} \tag{12}$$

The momentum equation of the water droplet is given as:

$$m\frac{Dv}{D\tau} + v\frac{Dm}{D\tau} = \sum F \tag{13}$$

Where $\sum F$ is the summation of the effective forces on the droplet, i.e.

$$\Sigma F = F_1 - F_2 - F_3 \tag{14}$$

So, the momentum equation of the water droplet leaving the nozzle is written as:

$$\begin{aligned} &\frac{\pi d^3 \rho_w Dv_w}{6D\tau} + \frac{(v_w - v_v) D (\frac{\pi}{6} d^3 \rho_w)}{D\tau} = \\ &\frac{g\pi d^3 \rho_w}{6} - \frac{\pi g d^3 \rho_v}{6} - \frac{C_D \pi d^2 \rho_v (v_w - v_v)^2}{8} \end{aligned} \tag{15}$$

The vapor velocity can be neglected compared with the sprayed water velocity, Ibrahim [8], i.e. $v_v \approx 0.0$ then, Equation (15) can be rewritten as:

$$\frac{Dv_w}{D\tau} = \frac{(\rho_w - \rho_v)g}{\rho_w} - \frac{3C_D\rho_v}{4\rho_w}\frac{v_w^2}{d} - \frac{v_w}{d^3}\frac{Dd^3}{D\tau} \tag{16}$$

The term $\frac{Dd^3}{D\tau} = 3d^2\frac{Dd}{D\tau}$, then equation (16) is reduced to:

$$\frac{Dv_w}{D\tau} = \frac{(\rho_w - \rho_v)g}{\rho_w} - \frac{3C_D\rho_v}{4\rho_w}\frac{v_w^2}{d} - \frac{3v_w}{d}\frac{Dd}{D\tau} \tag{17}$$

The change rate of droplet diameter ($\frac{Dd}{D\tau}$) can be obtained from the following equation, Lekic and Ford [9]:

$$\frac{Dd}{D\tau} = \frac{2\pi^2\alpha\varepsilon}{d_l}\frac{e^{-\pi^2 f_o}}{(1-e^{-\pi^2 f_o})^{1/2}} \tag{18}$$

where:

$$\varepsilon = (1+cp_w(\frac{t_s - t_{w1}}{LH})^{1/3}) - 1 \tag{19}$$

$$\alpha = \frac{k_w}{\rho_w cp_w} \tag{20}$$

$$f_o = \frac{4(\tau_2 - \tau_1)\alpha}{d_1^2} \tag{21}$$

The change of droplet diameter during condensation can be solved from the following equation, Lekic and Ford [9]:

$$d = d_1[1+\varepsilon(1-e^{-\pi^2 f_o})^{\frac{1}{2}}] \tag{22}$$

By solving Equations (17), (18) and (22), then the droplet velocity (v) can be estimated in terms of droplet initial diameter (d_1), droplet initial velocity (v_1), droplet initial temperature (t_1) and saturation temperature (t_s).

During the contact of water droplets with the vapor, heat is transferred between the two phases and the droplet temperature (t_2) at distance ZZ from the nozzle can be calculated from the following equation, Lim et al. [10]:

$$t_2 = \frac{1}{cp_w}[\frac{d_l^3(cp_w t_w - h_v)}{d^3} + h_v] \tag{23}$$

where the enthalpy of vapor (h_v) is a function of the evaporation pressure.

3.3. The region around the heated tube surface

As shown in Fig. (6), due to the spraying of water, a thin film of it is formed around the horizontal tube. The tube wall temperature is assumed to be constant and denoted as t_w and also the saturation temperature of the falling water t_s corresponding to the surrounding pressure. Also, in this evaluation the coordinates (r,θ) are used. The average water film tangential velocity and the film thickness are denoted as v' and δ respectively.

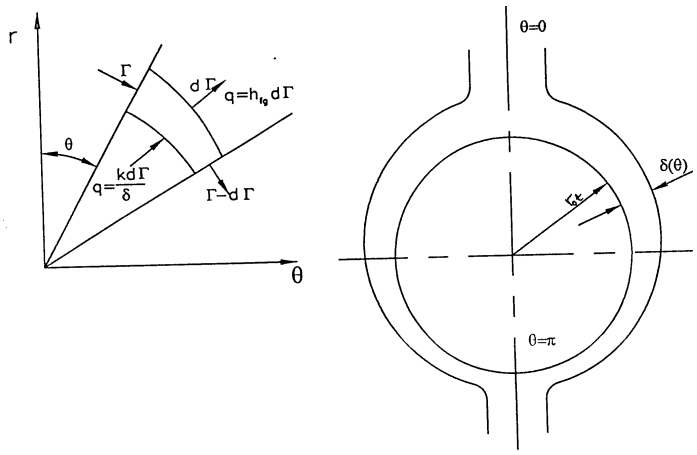

Fig. (6). Heat balance of a general element.

3.3.1 Governing equations

To simplify the describing equations of heat transfer process through the thin film some assumptions were made as:

- Conduction heat transfer takes place in radial direction (r-direction) while heat transfer by convection is assumed in the tangential direction (θ-direction).
- The flow around the tube is assumed to be one directional flow in tangential direction.
- The wall temperature is constant and uniform.
- The entire tube surface is covered with liquid film; (there is perfect wetting).
- The film flow is laminar, steady and ideal.
- The film thickness is small compared to the tube diameter.
- There is no nucleate boiling within the film.
- Evaporation occurs on the liquid-vapor interface where the temperature is at saturation.
- The surface tension effect is negligible.

According to the foregoing assumptions the continuity, momentum and energy equations in the cylindrical coordinates are simplified to the following forms:

$$\frac{1}{r}\frac{(\partial ru)}{\partial r}=\frac{1}{r}\frac{(\partial v)}{\partial \theta}-\frac{\partial w}{\partial z}=0 \tag{24}$$

$$\frac{v}{r}\frac{\rho}{\partial \theta}\frac{(\partial v)}{\partial \theta}=g(\rho_w-\rho_v)\sin(\theta)+\mu_w[\frac{1}{r}\frac{\partial}{\partial r}(r\frac{\partial v}{\partial \theta})+\frac{1}{r^2}\frac{\partial v^2}{\partial \theta^2}] \tag{25}$$

$$\rho cp\frac{v}{r}\frac{\partial t}{\partial \theta}=k_f[\frac{1}{r}\frac{\partial}{\partial r}(r\frac{\partial t}{\partial r})+\frac{1}{r^2}\frac{\partial t^2}{\partial \theta^2}] \tag{26}$$

The boundary conditions are:

$$\begin{aligned} &\text{at } r=r_{ot} && v=0, && t=t_w \\ &\text{at } r=r_{ot}+\delta(\theta) && \frac{\partial v}{\partial r}=0, && t=t_s \end{aligned} \tag{27}$$

Where, δ (θ) is the film thickness around the tube at the angular position (θ).

3.3.2 Estimation of film thickness

In order to estimate the film thickness, as a first approximation used to obtain the first solution of the governing equations, the temperature profile is assumed to be linear. Also, the heat transfer from the hot surface to the sprayed liquid is due to conduction only. Thus, the overall energy balance of the element can be made. This is carried out by assuming that heat is conducted across the film in the radial direction and evaporation takes place at the free surface. Also, the viscous force in tangential direction is taken in account, while that in radial direction is negligible. Furthermore, the inertia terms in radial and axial directions are neglected and the derivative of velocity that respect to θ direction can be neglected.

Thus the mean velocity across the film thickness can be presented as:

$$v'=\frac{g(\rho_w-\rho_v)\sin(\theta)}{4\mu_w}r_{ot}\delta\sin(\theta) \tag{28}$$

The mass flow rate at any position can be determined by applying the conservation law of mass as:

$$\Gamma=\rho_w v'\delta(\theta) \tag{29}$$

where v' is the average film velocity and Γ is the mass flow rate per unit length per one side at any position of tube.

From Equations (28) and (29) the film thickness as a function of θ can be given as:

$$\delta(\theta)=[\frac{4\mu_w\Gamma}{r_{ot}g\rho_w(\rho_w-\rho_v)\sin(\theta)}]^2 \tag{30}$$

Assuming approximate value of δ(θ) to Equation (30) as a first guess then, Equations (26) to (29) can be solved numerically. In which the velocity and temperature distributions throughout the flow field can be obtained. Then, the overall heat balance of this element can be presented as:

$$-D\Gamma(LH) = k_f \left(\frac{t_w - t_s}{\delta}\right] rD\theta \tag{31}$$

Accordingly, $\Gamma_o(\theta = 0.0)$ is the mass flow rate of the falling film per one side per unit length of tube.

Equation (30) can be rewritten as:

$$\delta_n(\theta) = \left[\frac{-k(t_w - t_s) rD\theta}{h_{fg} D\Gamma}\right]^2 \tag{32}$$

where $\delta_n(\theta)$ is noted as the improved value for the film thickness. If the result of the comparison between the improved value of the film thickness $\delta_n(\theta)$ and the approximate value of $\delta(\theta)$ is not satisfactory, the foregoing steps of the solution are repeated till; the error is within allowable prescribed value.

3.3.3 Average heat transfer coefficient and the evaporation rate

The local heat transfer coefficient and local Nusselt number can be determined according to the following equations:

$$h_o = \frac{q_w}{t_w - t_s} = \left(\frac{-k_f}{t_w - t_s}\right)\left[\frac{\partial t}{\partial r}\right]_{r=r_{ot}} \tag{33}$$

$$Nu = \frac{h_o d_{ot}}{k_f} \tag{34}$$

and the average heat transfer coefficient (h') is given as:

$$h' = \frac{1}{\pi}\int_0^{\pi} h_o D\theta \tag{35}$$

The evaporation rate can be calculated as:

$$m'_{ev} = \frac{hA_{ot}(t_w - t_s)}{cp_1(t_s - t_1) + LH} \tag{36}$$

where,

$$A_{ot} = \pi\, d_{ot}\, L \tag{37}$$

Then, the amount of evaporation rate (m'_{ev}) can be calculated from Equation (37). From which, the amount of the falling mass flow rate to the second tube ($m'_{ws.2}$), can be calculated as:

$$m'_{ws.2} = m'_{ws\cdot 1} - m'_{ev} \tag{38}$$

Then, the liquid film thickness, average heat transfer coefficient and evaporation rate for the second tube inline can be evaluated. Also, the mass flow rate inline to the third tube can be calculated by the same previous procedure. And so on for the next inline tubes in the bundle.

The evaporation rate ratio for the bundle can be calculated from the following equation:

$$\eta_{ev} = \frac{1}{m'_{ws.1}} \sum_{i=1}^{i=n_t} m'_{ev.i} \tag{39}$$

Where, n_t is the number of tubes inline in the bundle, and $m'_{ws.1}$ is the mass flow rate to the first vertical tube in the bundle.

3.3.4 Numerical method for solving the liquid film thickness, heat transfer coefficient and Nusselt number

The obtained governing Equations (24) to (26) are solved numerically using finite difference technique. Hence, the differential equations are approximated by a set of simultaneous linear equations. The Gauss-Seidel iterative method is applied to solve these equations. The numerical solution of the equations is carried out in successive manner, i.e. the obtained solution of the equations at certain cross section (certain value of radius r) is dependent upon the previously obtained value of the cross section (preceding the radius r) and so on. Knowing the temperature and velocity flow field, the value of the local and average heat transfer coefficient can be calculated.

4. RESULTS AND DISCUSSIONS

4.1. Effect of radial distance from the spray centerline on the formed droplet velocity and size

Figure (7) illustrates the effect of the radial distance from the spray centerline on droplet sauter mean diameter (d_{32}), droplet mass mean diameter (d_{30}) and droplet mean velocity (v_m) at different spray pressures and at an axial distance of 24 cm.

From Figures (7a) and (7b) respectively, it can be seen that, the droplet size increases by increasing the radial distance from the spray centerline. This is due to the great

effect of the inertia force at the spray centerline and the effect of the drag force at the spray periphery. Also, from Figure (7c), it can be seen that, the droplet mean velocity has a maximum value at the spray center line, and decreases towards the edge of the spray due to the effect of the inertia force at the spray centerline and the great effect of the drag force of the surrounding medium at the spray periphery.

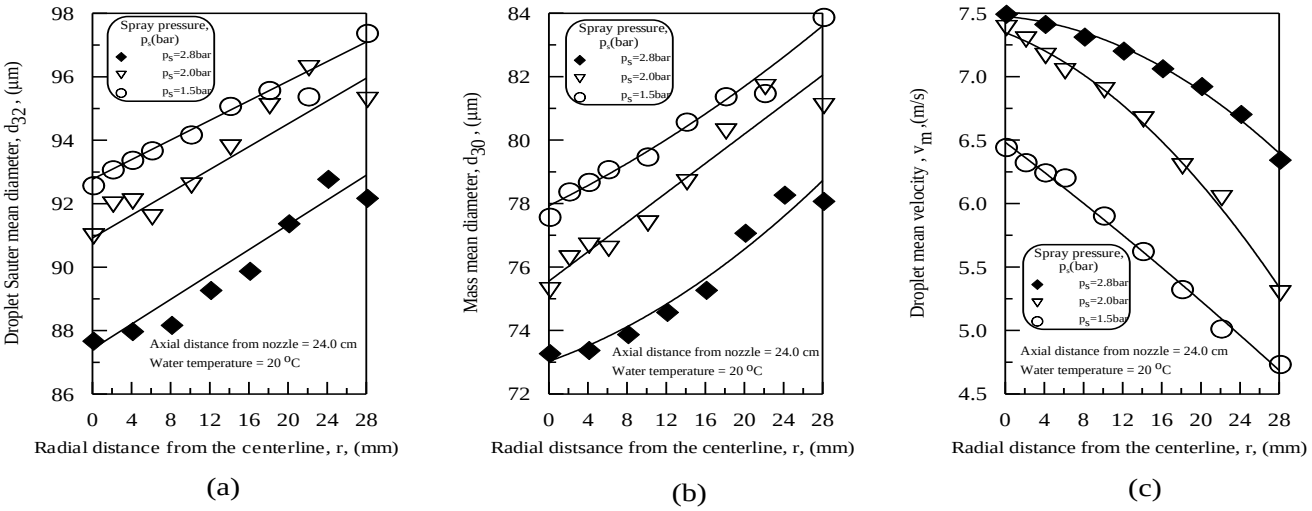

Fig. (7). Change of droplet sauter mean diameter, droplet mass mean diameter and droplet mean velocity with change of radial distance from the centerline of the nozzle at different values of the spray pressure.

4.2. Effect of axial distance from the spray nozzle on the formed droplet velocity and size

The effect of axial distance from the spray nozzle on the droplet velocity and size is represented in Fig. (8). As seen in Figures (8a) and (8b), the sauter mean diameter and the mass mean diameter decrease with increasing the axial distance from the nozzle. That is due to secondary atomization near the nozzle exit and droplet entrainment and migration, from the surrounding medium, further downstream.

Also, from Figure (8c) it can be seen that, the droplet mean velocity decreases by increasing the axial distance from the nozzle due to the effect of drag force from the surrounding medium. Also, the Sauter mean diameter and the mass mean diameter decrease with the increase in spray pressure. While the increase in spray pressure increases the droplets mean velocity.

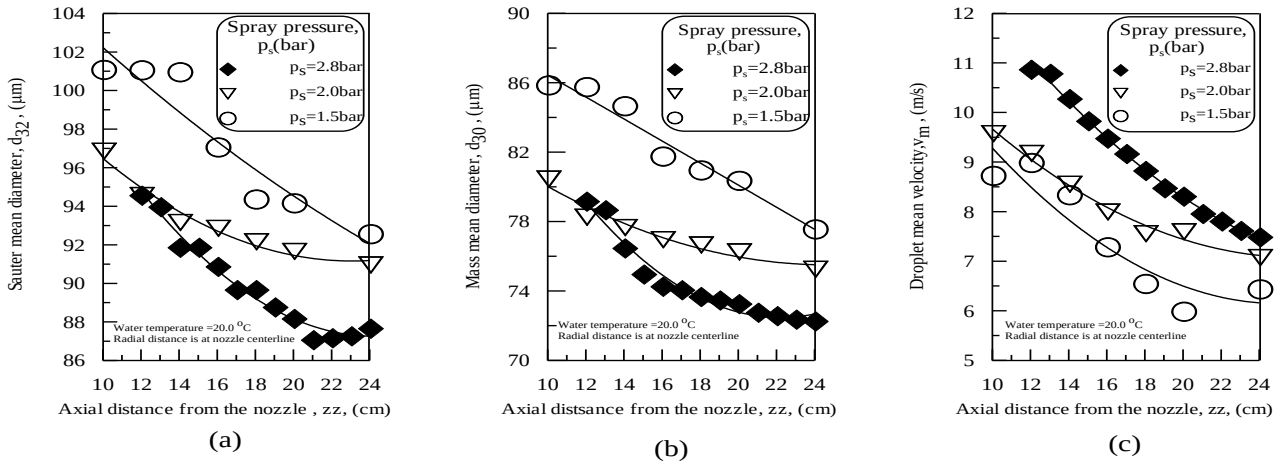

Fig. (8). Change of droplet sauter mean diameter, droplet mass mean diameter and droplet mean velocity with change of axial distance from the nozzle at various values of the spray pressure.

4.3. Effect of falling distance on the layer thickness and Nusselt number for different initial sprayed subcooling

Figure (9a) shows that, as the droplet falling distance ratio (zz/zz_{max}) increases, the water layer thickness ratio (δ/d_{ot}) increases, [Equation (32)]. Also, the water layer thickness is increased by increasing the subcooling It can also be seen that, for the high value of the inlet water subcooling ratio $(t_s - t_1)/t_s$

Figure (9b) shows that, increasing the droplet falling distance ratio decreases Nusselt number, Equation (34). Also, increasing the sprayed subcooling, decreases Nusselt number. That is due to the increase of the water layer thickness [Fig. (9a)] in which it tends to reduce the heat transfer from the hot tube surface to the sprayed water.

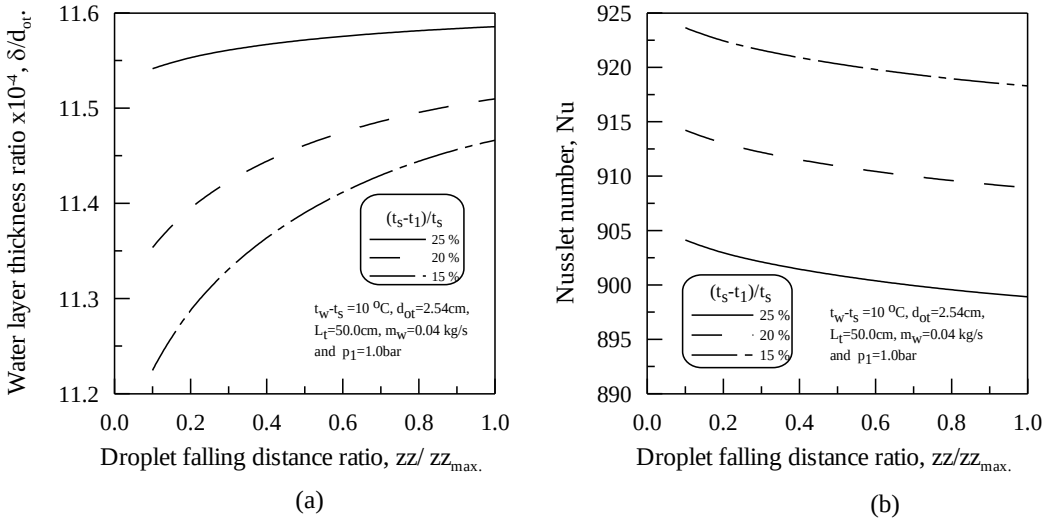

Fig. (9). Effect of falling distance on water layer thickness and Nusselt number at different values of water initial subcooling.

4.4. Effect of evaporation pressure on the water layer thickness and Nusselt number

Figure (10a) illustrates the increase of the water layer thickness ratio (δ/d_{ot}) [obtained from Equation (32)] with increasing the droplet falling distance ratio (zz/zz_{max}) at different values of chamber pressure (p_1). This is because, the temperature difference between the hot surface and the saturation temperature of the formed vapor will decrease by increasing the chamber pressure then, the formed water layer thickness ratio around the hot surface will increase. According to Equation (34) and Figure (10b), the Nusselt number decreases by increasing both of the chamber pressure and the falling distance or increasing one of them.

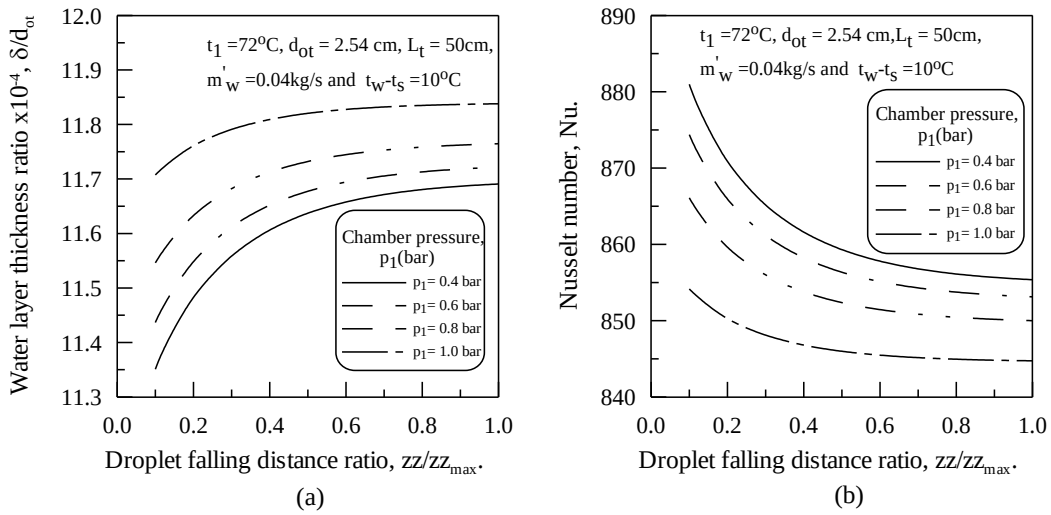

Fig. (10). Change of water layer thickness and Nusselt number against the falling distance at different values of chamber pressure.

4.5 Effect of angular position on the film thickness around the hot surface and on Nusselt number

The falling film thickness ratio (δ/d_{ot}) and Nusselt number (Nu) around the hot tube for different inline vertical bundle tubes at different angular positions are presented in Figure (11). It is shown that, the falling film thickness reaches its maximum value at the top angular position, [at $\theta = 0$, Figure (6)]. This thickness decreases from position at $\theta = 0$ to $\theta = \pi/2$ and then increases again up to $\theta = \pi$. Also, the film thickness ratio that is formed around the upper tube is greater than that formed around lower tubes located in the same vertical column. This is because the falling mass flow rate to the upper tube is greater than the falling mass flow rate to the lower tubes due to the evaporation from the upper tubes.

Basically, the Nusselt number decreases by increasing the film thickness ratio around the hot tube surface so, the local Nusselt number has its maximum value at the

tangential position of $\pi/2$ and it decreases rapidly towards $\theta = 0$ and $\theta = \pi$. Furthermore, the local Nusselt number at the upper tube is less than that at the lower tubes.

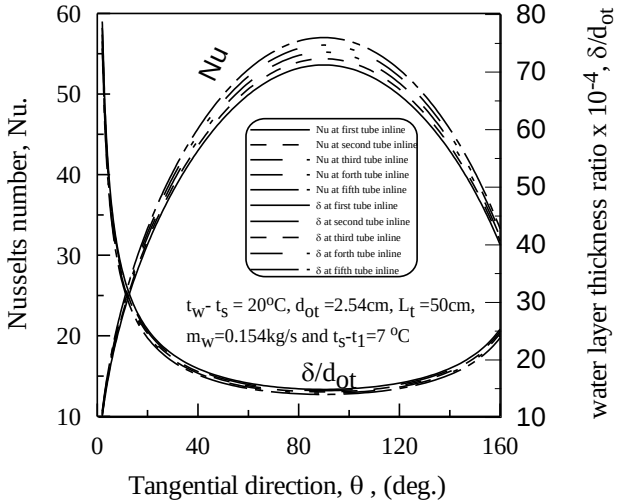

Fig. (11). Change of water layer thickness and Nusselt number against the tangential direction of the hot tube for different rows of the tube bundle.

4.6. Effect of the hot surface temperature on the film thickness around the hot tubes and Nusselt number

Figure (12a) shows that, the formed film thickness ratio (δ/d_{ot}) decreases by increasing the hot tube surface temperature difference ($t_w - t_s$). This is due to the increase of the evaporation rate as a result of increasing the hot surface temperature. Also from that figure, the film thickness ratio (δ/d_{ot}) decreases by increasing the hot tube surface temperature difference ($t_w - t_s$), as discussed above.

From Figure (12b), it can be seen that Nusselt number on the upper tube is less than that on the lower tube inline. This is attributed to the small film thickness that exists on the lower tubes. Furthermore, Nusselt number increases as the hot tube surface temperature difference increases also, due to the decrease of the film thickness.

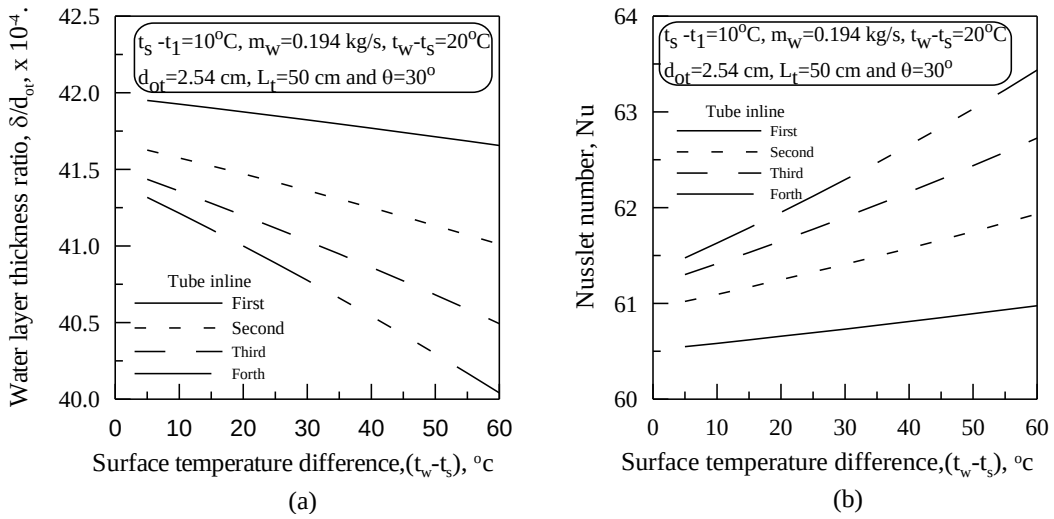

Fig. (12). Change of water layer thickness and Nusselt number against the surface temperature difference for different rows of the tube bundle.

4.7. Effect of the hot surface temperature on the evaporation rate with the change of the initial sprayed mass flow rate

Figure (13a) shows that, increasing the surface temperature difference ($t_w - t_s$) decreases the water layer thickness ratio (δ/d_{ot}), Equation (32). And it can also be seen that, for the high value of the initial sprayed mass flow rate per unit length per one side of the tube (Γ), there is a high value of the water layer thickness ratio and vice versa.

Figures (13b) and (13c) respectively show that Nusselt number (Nu) obtained from Equation (34) and evaporation rate ratio (η_{ev}) obtained from Equation (39) increase as increasing the surface temperature difference temperature ($t_w - t_s$). It can also be seen that, Nusselt number and the evaporation rate ratio are inversely proportional to the initial sprayed mass flow rate per unit length per one side of the tube (Γ). That is because, the liquid layer thickness around the hot tube surface increases by increasing the initial sprayed mass flow rate per unit length per one side of the tube and it tends to reduce heat transfer from the hot tube surface to the sprayed liquid.

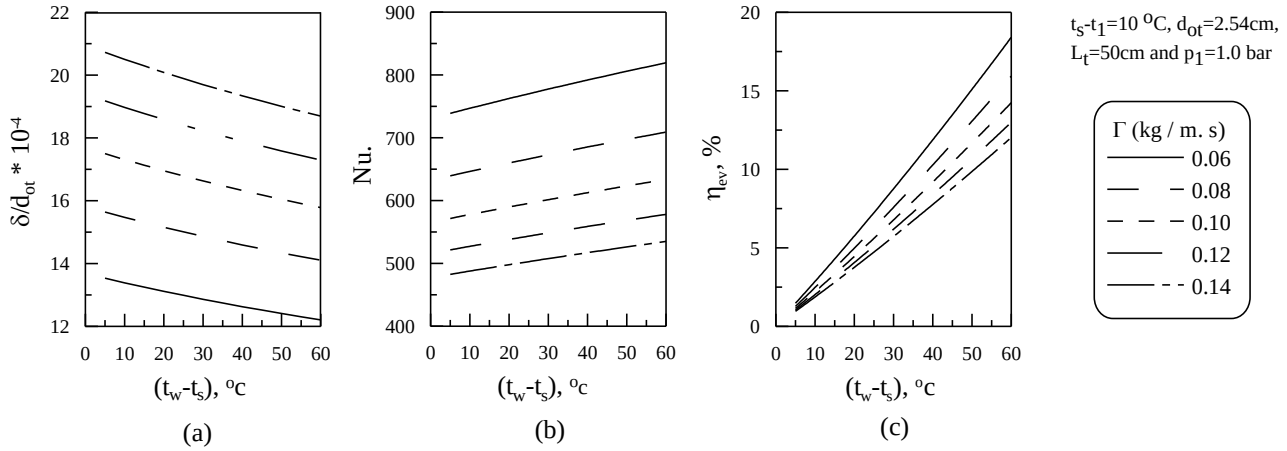

Fig. (13). Change of water layer thickness, Nusselt number and evaporation rate ratio against the surface temperature difference for different values of the initial sprayed flow rate.

4.8. Effect of the surface temperature on the evaporation rate with different tube outer diameters

Figure (14a) shows that, for small tube outer diameter the water layer thickness ratio is bigger than that for larger diameters. This is because the sprayed mass flow rate per unit length per one side of the tube (Γ) increases by decreasing the tube outer diameter.

As discussed above and from Figures (14b) and (14c), the Nusselt number (Nu) obtained from Equation (34) and evaporation rate ratio (η_{ev}) obtained from Equation (39) are increased as the surface superheating ($t_w - t_s$) is increased. From these figures, it can also be seen that, Nusselt number and the evaporation rate ratio are relatively proportional with the tube outer diameter.

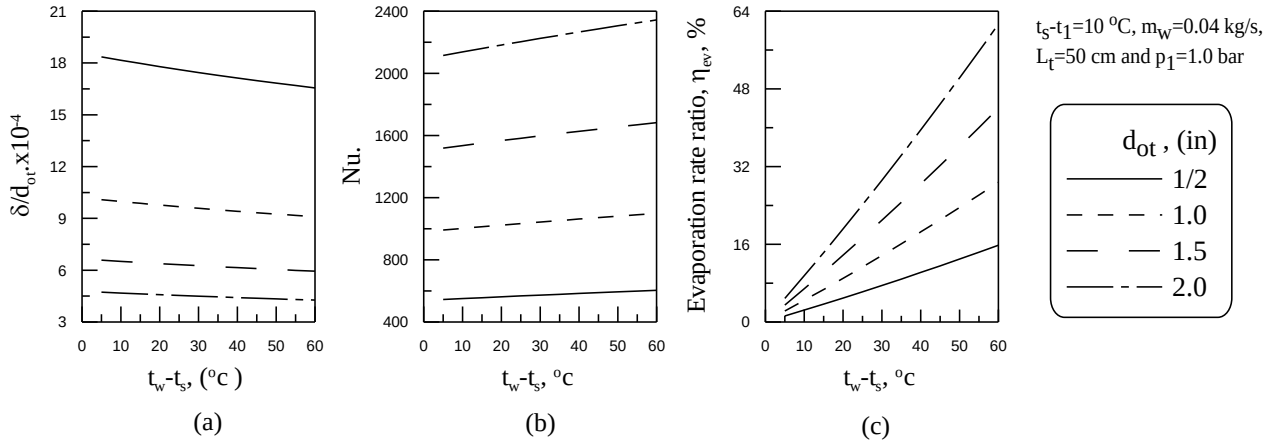

Fig. (14). Change of water layer thickness, Nusselt number and evaporation rate ratio against the surface superheating for different values of the hot tube outer diameter.

4.9. Comparison between the experimental and the theoretical results

4.9.1. Effect of the falling distance on the water film thickness around each tube of the bundle

Figure (15) illustrates the comparison between the theoretical and experimental results for the effect of the falling distance ratio (zz_t/d_{ot}) on the water layer thickness (δ) around the different rows of hot horizontal inline tubes. From this figure, it can be seen that, the water layer thickness increases as the falling distance increases. This is due to the condensation of part of the formed vapor around the sprayed droplet surface.

It can also be seen that, the water layer thickness around the lower tubes is less than that around the upper tubes. That is because, the falling water rate upon the lower tubes is less than that upon the upper tubes due to the evaporation which takes place at the upper tubes.

The difference between the experimental and theoretical results is in the range of 10 to 15%. This difference may be due to the following parameters which are not taken into consideration in the mathematical model; heat losses to the environment, entrainment and migration of the sprayed droplet further downstream by the formed vapor and the spattering of the sprayed water upon tube surface.

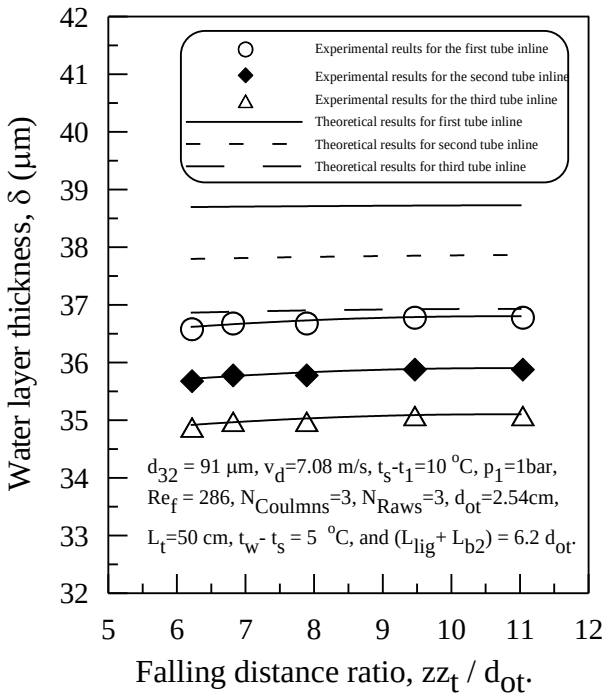

Fig. (15). Comparison between the theoretical and experimental results for the effect of the falling distance on the water film thickness.

4.9.2. Effect of the falling distance on the evaporation rate

Figure (16) illustrates a comparison between the experimental and the theoretical results for the effect of the falling distance ratio (zz_t/d_{ot}) on the evaporation rate ratio, for different values of the tube surface temperature difference.

From this figure, it can be seen that, the maximum evaporation rate ratio occurs at a falling distance ratio that is equivalent to the summation of water sheet breakup length and ligament breakup length which are depend on the working conditions. Less this distance, the evaporation rate ratio increases as the falling distance increases. This is due to the increase of the projected hot surface area and hence the increase of the transmitted heat from the hot surface to the formed water film. After this distance, the evaporation rate ratio decreases slightly with respect to the falling distance. This is related to the condensation of vapor on the sprayed droplet surface that increases as the falling distance increases. Therefore, inreacing the falling distance will increase the film thickness around the hot tube and hence reduces the heat transfer from the hot tube surface to the water film.It can also be seen that, the evaporation rate ratio increases as the surface temperature difference increases. This is due to the fact that the heat transfer from the hot tube surface to the water film increases as the surface temperature difference increases. The difference between the experimental and theoretical results ranges from 10 to 15%.

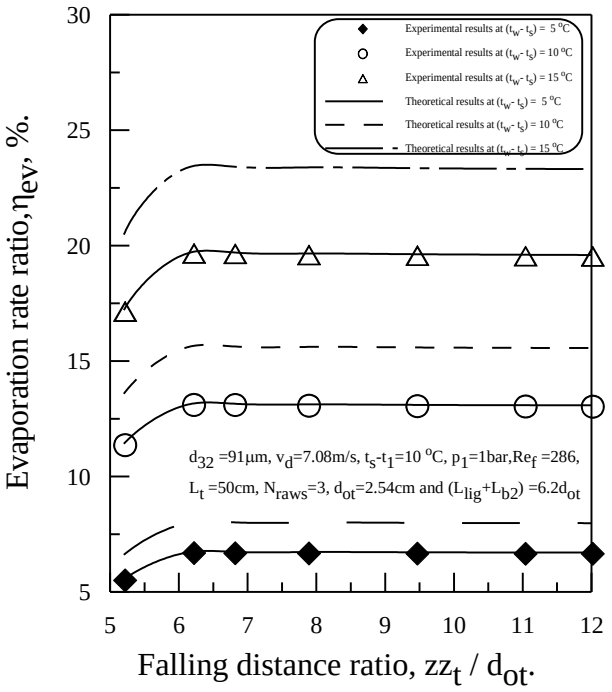

Fig. (16). Comparison between the theoretical and experimental results for the effect of the falling distance on the evaporation rate at different values of the surface superheating.

4.9.3. Effect of the falling water Reynolds number on the water film thickness

Figure (17) illustrates the comparison between the theoretical and experimental results for the effect of the falling water Reynolds number (Re_f) on the water layer thickness (δ) around the different rows of the tube bundle.

From this figure, it can be seen that, the water film thickness increases as the falling water Reynolds number increases. Also, as a result of the evaporation which takes place at upper tubes, the water film thickness around the lower tubes is less than that around the upper tubes. The difference between the experimental and theoretical results is in the range of 10 to 15%.

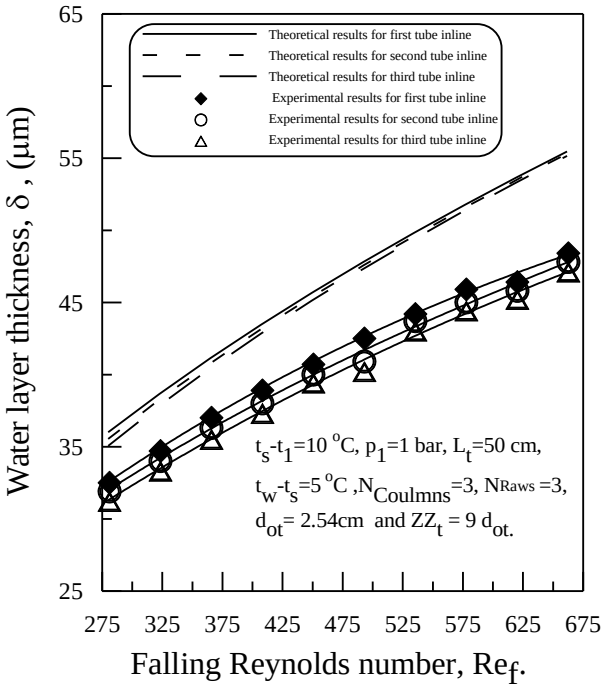

Fig. (17). Comparison between the theoretical and experimental results for the effect of the falling water Reynolds number on water film thickness.

4.9.4. Effect of the falling water Reynolds number on the evaporation rate

Figure (18) illustrates a comparison between the experimental and the theoretical results for the effect of the falling water Reynolds number (Re_f) on the evaporation rate ratio, (η_{ev}), for different values of the tube surface superheating.

From this figure, it can be seen that, the evaporation rate ratio decreases as the falling water Reynolds number increases. This is because, the formed water layer thickness around the hot surface increases by increasing the falling water Reynolds number and the increase in the initial sprayed mass flow rate per inline tube side. The increase in water layer tends to reduce the heat transfer between the hot tube surface and the

sprayed water. Also, the evaporation rate ratio increases as the surface temperature difference increases. This is due to that the transmitted heat from the hot tube surface to the water film layer increases as the surface temperature difference increases.The difference between the experimental and theoretical results is in the range of 10 to 15%. This difference can be attributed to the heat losses to the environment, spattering and water entrainment.

For $R_{ef} < 286$, all the sprayed water is evaporated and therefore, the water film around the hot tubes is unstable where, above this value the water film is stable.

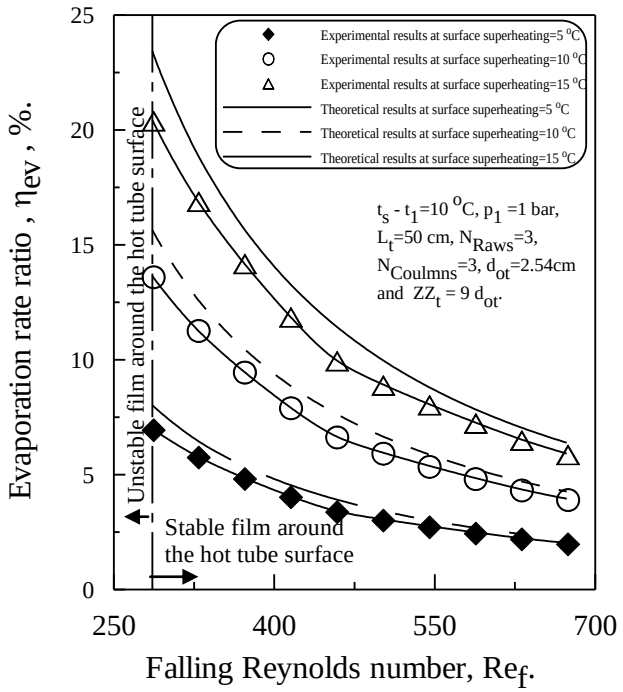

Fig. (18). Comparison between the theoretical and experimental results for the effect of the falling water Reynolds number on evaporation rate at different values of the surface superheating.

4.9.5. Effect of the falling water Reynolds number on the Nusselt number

Figure (19) illustrates a comparison between the experimental and the theoretical results for the effect of the falling water Reynolds number (Re_f) on Nusselt number, (Nu), at different values of the tube surface superheating.

From this figure, it can be seen that, Nusselt number decreases with the increase in falling water Reynolds number. This is because, the increase in the formed water layer thickness around the hot surface increases, which tends to resist the heat transfer from the hot tube surface to the sprayed water.

Also, Nusselt number increases as the surface temperature difference increases. The difference between the experimental and theoretical results is in the range of 10 to 15%.

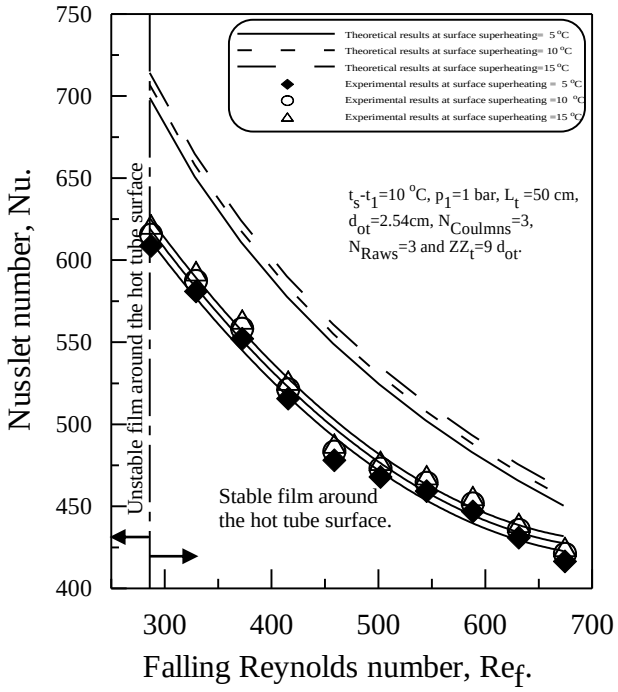

Fig. (19). Comparison between the theoretical and experimental results for the effect of the falling water Reynolds number on Nusselt number at different values of the surface superheating.

4.10. Experimental results for the effects of the falling distance and Reynolds number on Nusselt number

Figure (20) illustrates the experimental results for the effects of the falling distance ratio (zz/d_{ot}) and the falling Reynolds number (Re_f) on the Nusselt number (Nu), at different values of surface superheating.

From this figure, it can be seen that, the maximum Nusselt number occurs at a falling distance that is equivalent to the summation of distance of the liquid sheet breakup length and ligament breakup length. The breakup distances depend on the working conditions. Before the breakup, Nusselt number increases with the increase of the falling distance. After breakup, Nusselt number decreases slightly as the falling distance from the nozzle increases. This is due to the increase in condensation that takes place on the sprayed droplet surface with the increase in the falling distance. Hence, the formed water layer around the hot tube surface increases which will reduce the heat transfer from the hot tube surface to the water film.

It is noted that, the falling distance at which the maximum Nusselt number occurs decreases by increasing the falling Reynolds number. Increasing the surface superheating, also results in an increase in Nusselt number, since, the heat transfer from the hot tube surface to the water layer increases as the surface temperature increases. From the figure, it can be seen that, Nusselt number decreases with the increase in falling Reynolds number. This is due to the increase in the formed water layer thickness around the hot surface that tends to resist the heat transfer from the hot tube surface to the sprayed water.

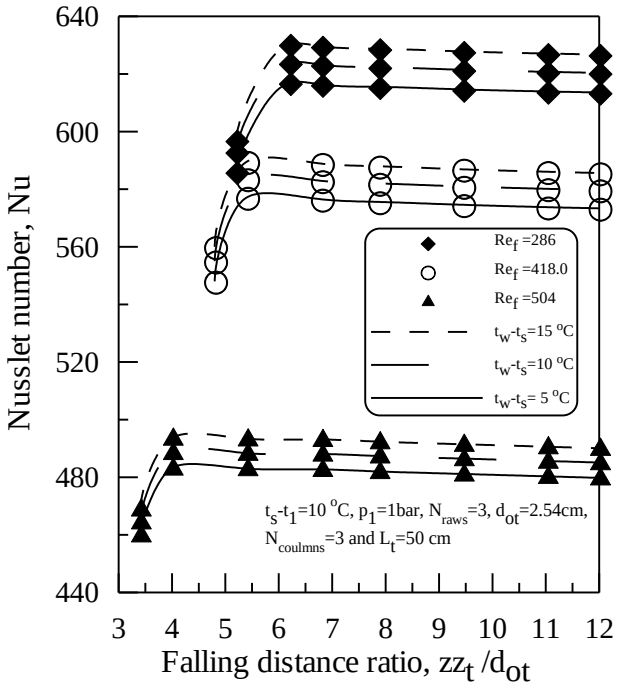

Fig. (20). Experimental results for effects of falling distance ratio and falling Reynolds number on the Nusselt number at different values of the surface superheating.

4.11. Dimensionless correlation for Nusselt number

Analysis of the experimental results enables achieving a relationship that describes the mechanism of heat exchange in the horizontal tube evaporators

The drawn correlation describes a relationship between the average heat transfer coefficient of the outside film and the following parameters; feed water rate, heat flux, falling distance from the nozzle to the hot tube surface, subcooling falling water temperature and the hot tube surface temperature. As the value of the falling distance, zz, is greater than the water sheet breakup length, L_{lig}, and the considered operating parameters were as:

- The transmitted heat flux from the hot tube surface ranged from 5.0 to 25.0 kW/m^2.

- Falling water Reynolds number ranged from 286 to 680.
- Falling distance ratio, the ratio between the falling distance from the nozzle and the hot tube outer diameter, raged from 4.0 to 12.
- The tube bundle is 3x3 tubes inline.
- Three flat-fan jet nozzles are used with spray pressure ranged from 1.5 to 3.5 bar.
- The droplet mean velocity is from 4.7 to 7.5 m/s, its sauter mean diameter is from 86.0 to 102.0 μm and its mass mean diameter is from 71.0 to 84.0 μm.
- The pressure inside the chamber is 1.0 bar and the temperature of the inlet water ranged from 90 to 93 °C.
- The temperature of hot tube surface ranged from 105.0 to 115.0 °C.
- The outer tube diameter is 2.54 cm and its length is 50.0 cm.

The final form for Nusselt number can be presented as:

$$Nu = 3321.534(Re_f)^{-0.4335}\,(Pr)^{0.121}(zz/d_{ot})^{-0.00023}\,(K_q)^{0.02271} \qquad (40)$$

Figure (21) determines the degree of agreement of the developed correlation with the experimental results. The figure shows that, the deviation between the predicted values and the experimental ones is in the range of –5.0 to 5.0%.

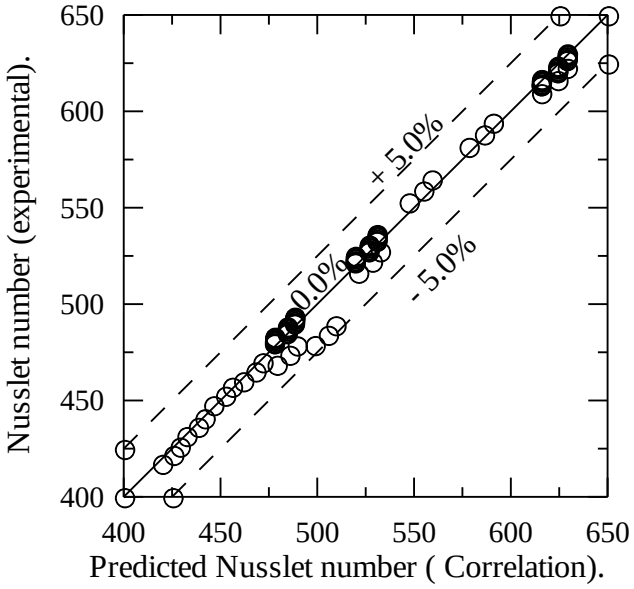

Fig. (21) Relationship between the experimental and the predicted results for Nusselt number.

CONCLUSIONS

From this study, the following conclusions can be drawn: The evaporation rate ratio and Nusselt number are mainly increased by increasing the surface superheating and

by increasing the tube outer diameter. Decreasing the chamber pressure, inlet liquid subcooling and sprayed mass flow rate result in increase of the evaporation rate and Nusselt number. There is an optimum value for the falling distance (which equal to the summation of water sheet breakup length and ligament brakup length), after this value, the falling distance has a little influence on the evaporation rate ratio and Nusselt number. Increasing the number of tubes in tube bundle increases the evaporation rate ratio but this number is restricted by the formed critical film thickness around the hot tubes. There is a reasonable agreement between the experimental and theoretical results. The validity of the predicted correlation is also very reasonable.

REFERENCES

1. Y. H. Wei and A. M. Jacobi, "Vapor-Shear, Geometric and Bundle- Depth Effects on the Inter Tube Falling-Film Modes", 1st International Conference on Heat Transfer, Fluid Mechanics, and Thermodynamics, 8-10 April 2002, Kruger Park, South Africa, (HEFAT 2002).
2. X. Hu and A. M. Jacobi, "Vapor-Shear, Geometric and Bundle- Depth Effects on the Inter tube Falling-Film Modes", The Inter Tube Falling Film: Part 1, Flow Characteristics, Mode Transitions and Hysteresis", Journal of Heat Transfer, Vol. 118, 1996, pp. 616-625.
3. N. Dombrowski and W. R. Johns, "The Aerodynamic Instability and Disintegration of Viscous Liquid Sheets", Chem. Eng. Sci., Vol. 18, pp. 201-214, 1963.
4. P. K. Senecal, D. P. Schmidt, I. Nouar, C. J. Rutland, R. D. Reitz, M. L. Corradini, "Modeling High-Speed Viscous Liquid Sheet Atomization", International Journal of Multiphase Flow, Vol. 25, 1999, pp. 1073-1097.
5. Fraser R. P., Eisenklam P., N. Domrowski and Hasson D., "Drop Formation From Rapidly Moving Sheets", AICHE J., Vol. 8, No. 5, 1962, pp. 672-680.
6. Lord Rayleigh, "On the Instability of Jets", Proc. Lond. Math. Soc., Vol. 10, pp. 4-13, 1879.
7. Jeremy D. M. Linn, Stephen, J. Maskell and Mike A. Patrick, "A Note on Heat and Mass Transfer to a Spray Droplet", Nuclear Technology, Vol. 81, pp. 122-125, APR. 1988.
8. N. A. Ibrahim, "Effectiveness of Containment Depressurization Spray Dystem in Nuclear Reactors", Ph.D. thesis, Zagazig university, 1989.
9. A. Lekic and J. D. Ford, "Direct Contact Concentration of Vapor on a Spray of Subcooled Liquid Droplets", Int. J. Heat Mass Transfer, Vol. 23, pp. 1531-1537, 1980.
10. I. S. Lim, R. S. Tankin and M. C. Yuen, "Condensation Measurements of Horizontal Steam/Water Flow", Journal of Heat Transfer, Vol. 106, pp. 425-482, May 1984.
11. M. M. Awad, E. R. Negeed, A. H. Mariy and M. M. Mahgoub, "Experimental Investigation of Spray Heat Exchanger Performance", Mansoura Engineering Journal, Vol. 32, pp. M1-M10, March 2007.

12. M. M. Awad, E. R. Negeed, A. H. Mariy and M. M. Mahgoub, "Computational Investigation of Spray Heat Exchanger Performance", Mansoura Engineering Journal, Vol. 32, pp. M11-M26, March 2007.